Industrial
Chemistry
& Materials

ROYAL SOCIETY
OF CHEMISTRY

PAPER

View Article Online
View Journal

Check for updates

Cite this: DOI: 10.1039/d5im00317b

Investigating the SO_2 absorption behavior of pyrimidine-based deep eutectic solvents *via* a dual-site thermodynamic model

Yiru Zou,[ac] Xiaoxiao Xing,[a] Chao Wang, [c] Duanjian Tao, *[d] Haiyan Ji,[c] Peiwen Wu, *[c] Yanhong Chao[a] and Wenshuai Zhu *[abc]

Received 6th November 2025,
Accepted 5th January 2026

DOI: 10.1039/d5im00317b

rsc.li/icm

Deep eutectic solvents (DESs), composed of hydrogen bond acceptors (HBAs) and hydrogen bond donors (HBDs), are widely used in flue gas desulfurization due to their excellent SO_2 absorption properties. In this work, 14 DESs with pyrimidine derivatives and their isomers (including 2-aminopyrimidine (AmPyr), 2-chloropyrimidine, 2-bromopyrimidine, 4-amino-2-hydroxypyrimidine, 2,4-dihydroxypyrimidine, 4,6-diaminopyrimidene, 2-aminopyrazine, and 3-aminopyridazine, respectively) as HBDs and 1-ethyl-3-methylimidazolium chloride (C_2mimCl) and 1-ethyl-3-methylimidazolium bromide as HBAs have been successfully prepared and used for SO_2 absorption. Among them, C_2mimCl-7 + AmPyr exhibited the highest SO_2 absorption (19.032 mol kg^{-1}, at 298.15 K and 1.0 bar), rapid gas–liquid equilibrium within 40 s, and an exceptional ideal selectivity of 528.7 for SO_2/CO_2. After 30 cycles of absorption–desorption, the SO_2 absorption capacity remained as high as 18.265 mol kg^{-1}. A dual-site reaction equilibrium thermodynamic model (DS-RETM) was established for absorption behavior analysis. Using C_2mimCl-7 + AmPyr as a case study, Henry's constant, equilibrium constants, and other thermodynamic parameters were determined. DS-RETM fitting further enabled visualization of the potential absorption behavior of each DES component, facilitating comparison of HBA and HBD effects on SO_2 absorption. This study offers new insights into the development of high-performance flue gas desulfurization absorbents and introduces a novel model for thermodynamic analysis of SO_2 absorption in DESs.

Keywords: Deep eutectic solvents; SO_2 absorption; Pyrimidine; Thermodynamic; Selectivity.

1 Introduction

The various fuels burned in factories during the production process, such as coal, oil, natural gas, *etc.*, will produce a large amount of flue gas.[1] The harmful gases contained therein, especially sulfur dioxide (SO_2), cause serious damage to the ecological environment and pose a significant threat to human health.[2] In the atmosphere, SO_2 oxidizes into sulfuric acid mist or sulfate aerosols, which are important precursors for environmental acidification. The content of SO_2 exceeding 0.5 ppm has potential impacts on human health, while when its concentration exceeds 1.5 ppm, healthy individuals may suffer from chronic bronchitis, laryngitis, and severe respiratory infections.[3,4] Thus, it is necessary to remove SO_2 before it is released into the atmosphere. Flue gas desulfurization (FGD) is the process of separating SO_2 from flue gas through various technologies and converting it into harmless or usable substances.[5] According to the state of the absorbent and product during the reaction process, it can be divided into wet, dry, and semi-dry desulfurization. Wet desulfurization technology is relatively mature, efficient, and easy to operate, and is the most widely used desulfurization method, including limestone gypsum method, ammonia absorption method, *etc.* However, these traditional absorbents have drawbacks such as irreversibility, volatility, and secondary environmental pollution.[6] Developing efficient, selective, and renewable absorbents is one of the key challenges in FGD technology.

Among all reported efficient absorbents, deep eutectic solvents (DESs) have been regarded as a promising one, because of their high selectivity, remarkable absorption

---

[a] *College of Chemical Engineering and Environment, State Key Laboratory of Heavy Oil Processing, College of Science, China University of Petroleum-Beijing, Beijing 102249, PR China. E-mail: zhuws@cup.edu.cn*
[b] *Shandong Key Laboratory of Green Electricity & Hydrogen Science and Technology, Shandong Institute of Petroleum and Chemical Technology, Dongying 257061, PR China*
[c] *School of Chemistry and Chemical Engineering, School of the Environment and Safety Engineering, School of Materials Science and Engineering, Jiangsu University, Zhenjiang 212013, PR China*
[d] *College of Chemistry and Chemical Engineering, Jiangxi Normal University, Nanchang 330022, PR China*

capacity, green characteristics, *etc.*[7] DESs were first proposed by Abbott in 2003 and are widely regarded as one of the green solvents.[8,9] They are formed by the interaction between hydrogen bond donors (HBDs) and hydrogen bond acceptors (HBAs) through hydrogen bonds, halogen bonds, or van der Waals forces, and have advantages such as easy synthesis, recyclability, designability, *etc.*[10–12] Due to the wide variety of HBDs and HBAs, theoretically, there could be at least 10^6 types of DESs, which can be designed with specific functions based on application requirements.[13] Since Han *et al.*[14] first used choline chloride-glycerol deep eutectic solvents to absorb SO_2 in 2013, various DESs have been developed for flue gas desulfurization. Among them, DESs using nitrogen-containing heterocyclic organic compounds as HBDs or HBAs, including imidazole,[15–18] triazole,[19] tetrazole,[20] benzimidazole,[21] pyrazole,[22] pyridine,[23–26] *etc.*, have been reported successively.

Pyrimidine, a six-membered nitrogen-containing heterocyclic organic compound, differs from pyridine in that it contains two alternating N atoms and has lower toxicity. Schröder *et al.*[1] reported that the N atom of the pyrimidine ring can form dipole–dipole interactions with the O atom in S═O, indicating that pyrimidine-based absorbents are excellent candidates for SO_2 absorption. However, the physical interaction formed by electrostatic attraction between polar molecules is relatively weak, which limits the ability of materials to remove SO_2. Notably, DESs prepared from pyridine derivatives containing functional groups such as $-NH_2$, –OH, and –COOH exhibit excellent SO_2 absorption capacity.[25,26] Thus, to prepare pyrimidine-based DESs with high SO_2 absorption performance, pyrimidine derivatives containing functional groups such as $-NH_2$, C═O, –Cl, and –Br have been inferred to enhance their interactions with SO_2.

Ulteriorly, to investigate the absorption behavior, the SO_2 absorption process of DESs was analyzed through a thermodynamic model. Zhang *et al.*[27] obtained the physical and chemical absorption enthalpy changes ($\Delta_r H_m$) of acidic protonic ionic liquid (APIL) based DESs through a reaction equilibrium thermodynamic model (RETM). In our previous work,[28] we also successfully used a RETM to demonstrate that purine-based DESs exhibit chemical absorption in the low-pressure region and physical absorption in the high-pressure region, and obtained a series of thermodynamic parameters. The absorption behavior of different DESs can be observed through the RETM, but how to gain more comprehensive insight into the absorption capacity of each component still needs further exploration.

In this work, a series of DESs with pyrimidine derivatives (one of 2-aminopyrimidine, 2-chloropyrimidine, 2-bromopyrimidine, 4-amino-2-hydroxypyrimidine, 2,4-dihydroxypyrimidine, and 4,6-diaminopyrimidene) or isomers of 2-aminopyrimidine (2-aminopyrazine or 3-aminopyridazine) as HBDs with 1-ethyl-3-methylimidazolium chloride or 1-ethyl-3-methylimidazolium bromide as HBAs have been successfully prepared. The relationship between temperature and the densities as well as viscosities of the prepared DESs was analyzed, and the thermal decomposition temperature (T_d) was further determined through thermogravimetric analysis. Subsequently, the SO_2 absorption performance of the prepared DESs was measured to investigate the effects of the molar ratio (HBAs : HBDs), HBD type, pressure, and temperature. Moreover, the time-dependent SO_2 absorption, SO_2/CO_2 selectivity and regeneration performance of pyrimidine-based DESs were also explored. Specifically, the physical and chemical absorption behavior of the prepared DESs was investigated using a dual-site reaction equilibrium thermodynamic model (DS-RETM), which can further elucidate the influence of HBAs and HBDs on SO_2 absorption and thermodynamic parameters. Finally, the possible interaction between pyrimidine-based DESs and SO_2 was further elucidated. Our findings offer a novel strategy for the design of high-performance, high-selectivity SO_2 absorbents and introduce a new thermodynamic model for SO_2 absorption in DESs.

2 Results and discussion

2.1 Characterization of pyrimidine-based DESs

The densities of the as-prepared DESs with C_2mimCl as a HBA were measured at different temperatures, as shown in Fig. 1a and b (Tables S1 and S2). Obviously, as the molar ratio increases from 2 : 1 to 7 : 1, the density of C_2mimCl-*n* + AmPyr DESs gradually decreases from 1.164 g cm^{-3} to 1.151 g cm^{-3} at 298.15 K. Thus, the increase of C_2mimCl is beneficial to decrease the density of C_2mimCl-*n* + AmPyr DESs. As for the DESs of C_2mimCl-7 + HBDs, the order of density (arranged by HBDs) at the same temperature is: AmPz < AmPd ≈ AmPyr < ChPyr < DAmPyr < Cyt < Ura < BrPyr. Considering that the molar ratio of C_2mimCl to HBDs remains unchanged, there exists a significant difference in density, indicating that the molecular structure of HBDs will affect the density of DESs significantly.[29] The density of DESs was fitted to the temperature (T) ($\rho_{\mathrm{DESs}} = \alpha + \beta T$, detailed parameters are provided in Tables S3 and S4). The results show that R_1^2 and R_2^2 are 0.999, revealing a linear relationship between densities and temperatures.

Subsequently, the viscosities of pyrimidine-based DESs were measured at different temperatures, as shown in Fig. 1c and d (Tables S5 and S6). The results in Fig. 1c are similar to the effect of temperature on densities, indicating that increasing C_2mimCl is beneficial for reducing its viscosities, which may be due to the formation of more intramolecular hydrogen bonds.[30,31] In Fig. 1d, the order of viscosities (at 298.15 K) for different C_2mimCl-7 + HBDs DESs is: C_2mimCl-7 + BrPyr < C_2mimCl-7 + ChPyr < C_2mimCl-7 + AmPz < C_2mimCl-7 + Ura < C_2mimCl-7 + AmPd < C_2mimCl-7 + AmPyr < C_2mimCl-7 + DAmPyr < C_2mimCl-7 + Cyt. Owing to the different types, positions, and numbers of functional groups in HBDs, their ability to form intramolecular hydrogen bonds with C_2mimCl differs from one another, demonstrating that the structures of HBAs and HBDs significantly alter the viscosities of DESs.[29] In addition, the viscosity of C_2mimCl-7 + AmPyr is higher than that of C_2mimBr-7 + AmPyr, which may be due to the

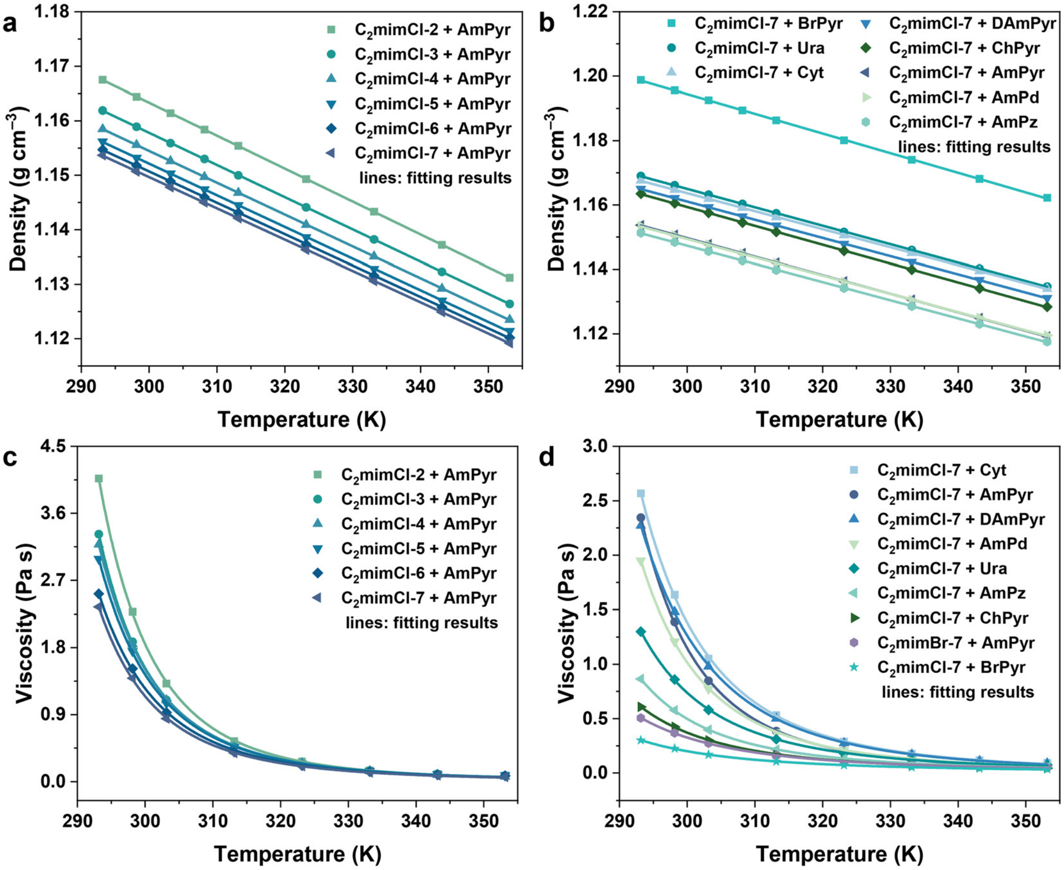

Fig. 1 The densities of (a) C_2mimCl-*n* + AmPyr (*n* = 2, 3, 4, 5, 6, 7) and (b) C_2mimCl-7 + HBDs; the viscosities of (c) C_2mimCl-*n* + AmPyr (*n* = 2, 3, 4, 5, 6, 7) and (d) HBAs-7 + HBDs.

different anions of HBAs, leading to the weaker ability of C_2mimBr and AmPyr to form intermolecular hydrogen bonds.[32] The viscosities were fitted to the temperature (T) (VFT equation: $\eta = \eta_0 \exp(t/(T - T_0))$,[33] and the detailed parameter data are shown in Tables S7 and 1). The results indicate that R_3^2 and R_4^2 are 0.999, suggesting an exponential relationship between viscosities and temperatures.

To investigate the thermal stability of pyrimidine-based DESs, HBAs-7 + HBDs were analyzed by thermogravimetry (TG), as shown in Fig. S1 and Table 1. Thermal decomposition temperature (T_d) can be used to judge the absorption temperature of absorbent and desorption temperature during regeneration, which is generally defined as the temperature at which the mass loss exceeds 5%. The maximum T_d value is 519 K (C_2mimCl-7 + AmPz), and the minimum value is 393 K (C_2mimCl-7 + BrPyr), indicating that pyrimidine-based DESs have excellent thermal stability during absorption–desorption processes and have the potential for flue gas desulfurization at high temperature.

2.2 SO_2 absorption of pyrimidine-based DESs

To explore the optimal molar ratio of HBAs to HBDs, the SO_2 absorption capacity of C_2mimCl-*n* + AmPyr was

Table 1 The viscosity fitting results and T_d of C_2mimCl-7 + HBDs

	HBDs								
Parameters	Cyt	AmPyr	DAmPyr	AmPd	Ura	AmPz	ChPyr	AmPyr*	BrPyr
$\eta_0 \times 10^4$ (Pa s)	6.591 ± 3.095	5.847 ± 2.319	4.233 ± 1.846	9.167 ± 3.933	13.50 ± 4.797	15.90 ± 3.597	12.20 ± 2.858	14.00 ± 8.586	18.60 ± 4.826
t_2 (K)	696.7 ± 83.61	601.2 ± 59.98	800.0 ± 85.88	563.1 ± 66.87	522.0 ± 58.61	448.2 ± 35.34	492.1 ± 41.15	495.7 ± 115.5	396.2 ± 46.08
T_0 (K)	208.9 ± 5.231	220.7 ± 3.644	200.0 ± 5.216	219.7 ± 4.482	217.2 ± 4.495	222.0 ± 2.981	214.0 ± 3.567	209.1 ± 10.69	215.4 ± 5.018
R_4^2	0.999	0.999	0.999	0.999	0.999	0.999	0.999	0.999	0.999
T_d (K)	508	443	503	514	503	519	464	444	393

AmPyr*: C_2mimBr-7 + AmPyr.

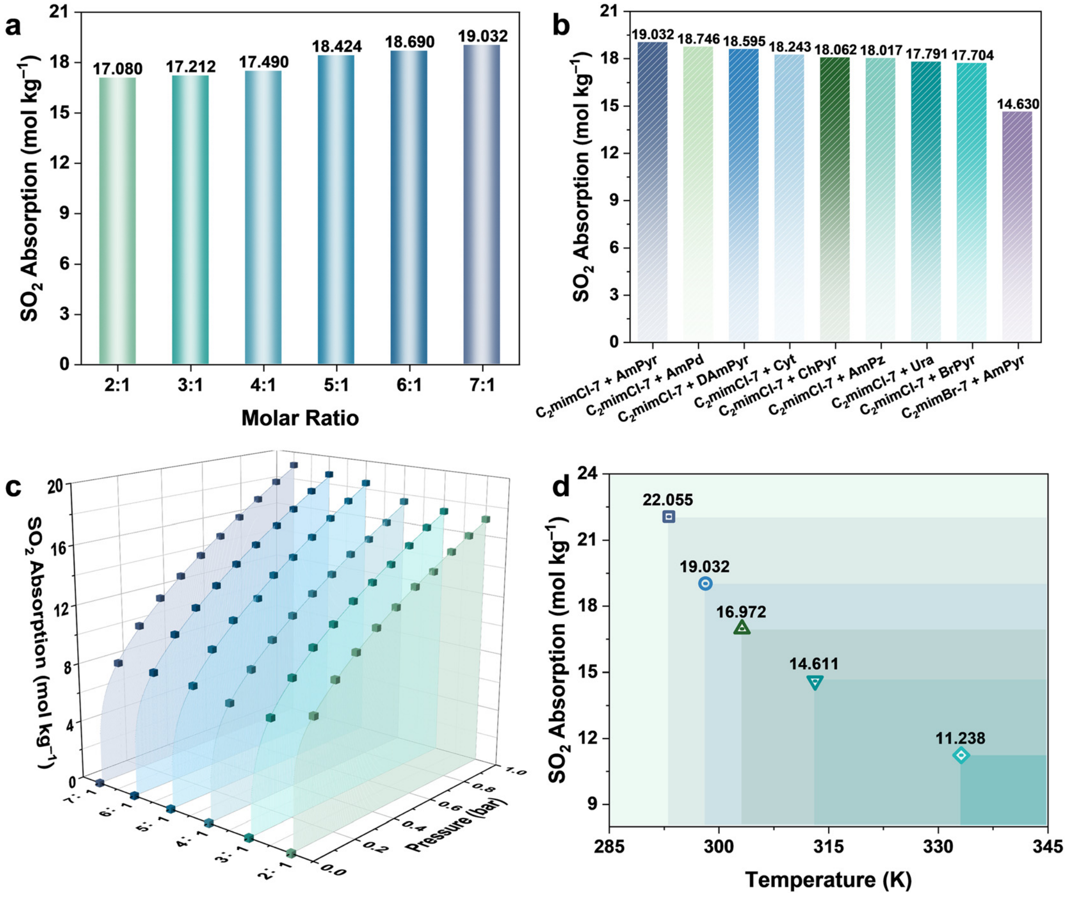

Fig. 2 The SO_2 absorption of (a) C_2mimCl-*n* + AmPyr and (b) HBAs-7 + HBDs, T = 298.15 K, P = 1.0 bar; (c) the effect of pressure on SO_2 absorption of C_2mimCl-*n* + AmPyr, T = 298.15 K; (d) the effect of temperature on SO_2 absorption of C_2mimCl-7 + AmPyr; P = 1.0 bar.

investigated. Fig. 2a shows the SO_2 absorption of C_2mimCl-*n* + AmPyr at 298.15 K and 1.0 bar. As the molar ratio of C_2mimCl to AmPyr increases, the SO_2 absorption of C_2mimCl-*n* + AmPyr increases gradually, reaching a maximum of 19.032 mol kg^{-1}. With the increase of C_2mimCl, the viscosity of C_2mimCl-*n* + AmPyr decreases, which is more beneficial to mass transfer;[34] nevertheless, the charge-transfer interaction between the highly electronegative Cl^- in C_2mimCl and the S atoms in SO_2 ($Cl^-\cdots SO_2$) is beneficial for improving SO_2 absorption.[35,36] According to the above analysis, the optimal molar ratio of C_2mimCl to AmPyr is 7 : 1.

Furthermore, a series of HBAs-7 + HBDs DESs were synthesized, and their SO_2 absorption capacity is shown in Fig. 2b. Besides, Table S8 shows the SO_2 absorption capacity of synthesized DESs compared to other materials, which are superior to many solid absorbents. For DESs with different HBAs, the absorption capacity of C_2mimBr-7 + AmPyr (14.630 mol kg^{-1}) is significantly lower compared to C_2mimCl-7 + AmPyr (19.032 mol kg^{-1}), indicating that anions have a greater influence on SO_2 absorption capacity. In other words, the greater the electronegativity, the higher the absorption capacity of SO_2.[29,32] As isomers of AmPyr, AmPd and AmPz were also used to form DESs with C_2mimCl. The SO_2 absorption capacities of C_2mimCl-7 + AmPz and C_2mimCl-7 + AmPd are 18.017 mol kg^{-1} and 18.746 mol kg^{-1}, respectively. These values, all lower than that of C_2mimCl-7 + AmPyr (19.032 mol kg^{-1}), demonstrate that the position of the nitrogen atoms within the heterocyclic ring structure of the HBDs also significantly impacts the performance of DESs, and the pyrimidine ring is more conducive to SO_2 absorption.

Hence, to develop pyrimidine-based DESs with superior performance, the SO_2 absorption of DESs using pyrimidine derivatives with different functional groups as HBDs was investigated. Firstly, with BrPyr, ChPyr, and AmPyr as HBDs, the SO_2 absorption capacity is C_2mimCl-7 + BrPyr < C_2mimCl-7 + ChPyr < C_2mimCl-7 + AmPyr. Typically, the higher the viscosity, the smaller the absorption capacity. Here, the main reason that affects the absorption capacity is that AmPyr contains weak basic functional groups ($-NH_2$), which may have acid–base interaction with SO_2 molecules.[37] Then, the SO_2 absorption of DESs with multifunctional pyrimidine derivatives (Ura, Cyt, and DAmPyr) as HBDs was further investigated. The SO_2 absorption of the three DESs is C_2mimCl-7 + Ura (17.791 mol kg^{-1}) < C_2mimCl-7 + Cyt (18.243 mol kg^{-1}) < C_2mimCl-7 + DAmPyr (18.595 mol kg^{-1}). Thus, the pyrimidine-based DESs with optimal SO_2 absorption is C_2mimCl-7 + AmPyr.

It is universally known that pressure plays a key role in affecting the gas absorption capacity of DESs.[38] Fig. 2c shows the SO_2 absorption of pyrimidine-based DESs at 298.15 K and 0–1.0 bar. The SO_2 absorption capacity of C_2mimCl-*n* + AmPyr increases nonlinearly with the increase of pressure. Taking C_2mimCl-7 + AmPyr with the highest absorption capacity as an example, with the pressure increasing from 0.1 bar to 1.0 bar, the absorption capacity of SO_2 increases from 7.911 mol kg^{-1} to 19.032 mol kg^{-1}. This shows that increasing the pressure can promote the absorption of SO_2. Conversely, reducing the pressure can be considered to desorb SO_2.[39,40] Additionally, the SO_2 absorption increases rapidly between 0 and 0.1 bar, probably owing to the chemical interaction between the absorbent and SO_2 molecules.[41] However, the growth rate of absorption capacity decreases between 0.1 and 1.0 bar, which may be due to the gradual occupation of absorption sites, so rapid absorption has been completed, resulting in the process being dominated by physical absorption. Therefore, it is speculated that the absorption process of SO_2 *via* pyrimidine-based DESs includes chemical absorption and physical absorption.[42]

According to the existing literature,[6,22,43–46] temperature is another important factor affecting the absorption capacity of DESs. Hence, C_2mimCl-7 + AmPyr was selected to investigate the SO_2 absorption performance at different temperatures, as shown in Fig. 2d. With the increase of temperature, the SO_2 absorption capacity of C_2mimCl-7 + AmPyr decreases continuously, and the absorption capacities are 22.055, 19.032, 16.972, 14.611 and 11.238 mol kg^{-1}, respectively. This result shows that increasing the temperature is beneficial to the regeneration of absorbent. Furthermore, it should be noted that C_2mimCl-7 + AmPyr still has a high absorption capacity at high temperatures, indicating that pyrimidine-based DESs could be used as candidate absorbents for high-temperature flue gas desulfurization.[29]

2.3 Analysis of SO_2 absorption behavior for pyrimidine-based DESs

A DS-RETM equation was established for fitting the SO_2 absorption.[47] It is assumed that the absorption of SO_2 by C_2mimCl-7 + AmPyr DESs involves the following steps:

$$SO_2\ (g) \rightarrow SO_2\ (l) \tag{1}$$

$$SO_2\ (g) + C_2mimCl\ (l) \rightarrow C_2mimCl\text{–}SO_2\ (l) \tag{2}$$

$$SO_2\ (g) + AmPyr\ (l) \rightarrow AmPyr\text{–}SO_2\ (l) \tag{3}$$

where g and l stand for gaseous and liquid states, respectively. C_2mimCl–SO_2 stands for the interaction of C_2mimCl with SO_2, and AmPyr–SO_2 stands for the interaction of AmPyr with SO_2. Eqn (1) denotes the physical absorption process and could be described by the following equation:

$$P = H{\cdot}\gamma_{SO_2}{\cdot}\frac{m_{\text{phys-SO}_2}}{m^\circ} \tag{4}$$

where P is the pressure (bar) of SO_2 (g); H is the Henry's law constant with the same unit as P; $m_{\text{phys-SO}_2}$ is the physical absorption molality (mol kg^{-1}); γ_{SO_2} is the activity coefficient; m° is 1.0 mol kg^{-1}. Eqn (2) and (3) denote the chemical absorption process and could be described by following equations:

$$k_{C_2\text{mimCl}} = \frac{\gamma_{C_2\text{mimCl–SO}_2}{\cdot}\frac{m_{C_2\text{mimCl–SO}_2}}{m^\circ}}{\frac{P}{P^\circ}{\cdot}\gamma_{C_2\text{mimCl}}{\cdot}\frac{m_{C_2\text{mimCl}}}{m^\circ}} \tag{5}$$

$$m^\circ_{C_2\text{mimCl}} = m_{C_2\text{mimCl–SO}_2} + m_{C_2\text{mimCl}} \tag{6}$$

$$k_{\text{AmPyr}} = \frac{\gamma_{\text{AmPyr–SO}_2}{\cdot}\frac{m_{\text{AmPyr–SO}_2}}{m^\circ}}{\frac{P}{P^\circ}{\cdot}\gamma_{\text{AmPyr}}{\cdot}\frac{m_{\text{AmPyr}}}{m^\circ}} \tag{7}$$

$$m^\circ_{\text{AmPyr}} = m_{\text{AmPyr–SO}_2} + m_{\text{AmPyr}} \tag{8}$$

$$m^\circ_{C_2\text{mimCl}} = \frac{1}{M_{C_2\text{mimCl}}} \tag{9}$$

$$m^\circ_{\text{AmPyr}} = \frac{1}{M_{\text{AmPyr}}} \tag{10}$$

where $k_{C_2\text{mimCl}}$ and k_{AmPyr} stand for the equilibrium constants; $\gamma_{C_2\text{mimCl–SO}_2}$, $\gamma_{C_2\text{mimCl}}$, $\gamma_{\text{AmPyr–SO}_2}$, and γ_{AmPyr} are the activity coefficients; $m_{C_2\text{mimCl–SO}_2}$, $m_{C_2\text{mimCl}}$, $m_{\text{AmPyr–SO}_2}$, and m_{AmPyr} are the molality (mol kg^{-1}); P° is 1.0 bar; $m^\circ_{C_2\text{mimCl}}$ and m°_{AmPyr} are constants (mol kg^{-1}) that could be calculated using eqn (9) and (10); $M_{C_2\text{mimCl}}$ and M_{AmPyr} are the molar mass of C_2mimCl and AmPyr, respectively, in g mol^{-1}.

The values of γ_{SO_2}, $\gamma_{C_2\text{mimCl–SO}_2}$, $\gamma_{C_2\text{mimCl}}$, $\gamma_{\text{AmPyr–SO}_2}$, and γ_{AmPyr} are all regarded as 1.0.[28,48] Thus, the DS-RETM could be expressed by eqn (11) and (12):

$$m_t = m_{\text{phys-SO}_2} + m_{\text{CmimCl–SO}_2} + m_{\text{AmPyr–SO}_2} \tag{11}$$

$$m_t = \frac{P}{H} + \frac{k_{C_2\text{mimCl}}{\cdot}P{\cdot}m^\circ_{C_2\text{mimCl}}}{k_{C_2\text{mimCl}}{\cdot}P + 1} + \frac{k_{\text{AmPyr}}{\cdot}P{\cdot}m^\circ_{\text{AmPyr}}}{k_{\text{AmPyr}}{\cdot}P + 1} \tag{12}$$

where m_t (mol kg^{-1}) is the total SO_2 absorption.

The SO_2 absorption of C_2mimCl-7 + AmPyr at different temperatures and pressures was correlated according to eqn (12), and fitted lines are shown in Fig. 3a. Notably, the fitting curve matches well with the experimental data, with R_5^2 values greater than 0.999, indicating that the established thermodynamic model has extremely high reliability. The corresponding fitting parameters were calculated and revealed in Table 2. The Henry's law constants keep an increasing trend, while the equilibrium constants keep a decreasing trend, which is consistent with the negative dependence of SO_2 absorption on temperature.

Based on the H, $k_{C_2\text{mimCl}}$, and k_{AmPyr}, the $m_{\text{phys-SO}_2}$, $m_{C_2\text{mimCl–SO}_2}$ and $m_{\text{AmPyr–SO}_2}$ could be obtained. As shown in Fig. 3b and c, both physical absorption and chemical absorption decrease with increasing temperature. The

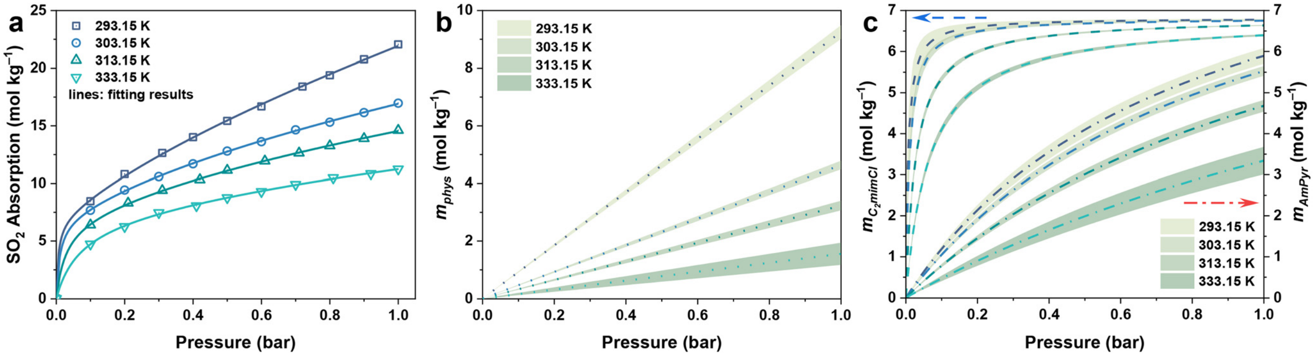

Fig. 3 (a) DS-DETM equation fitting of C_2mimCl-7 + AmPyr for SO_2 absorption; the calculated (b) physical and (c) chemical absorption of SO_2 by C_2mimCl-7 + AmPyr.

Table 2 Calculated Henry's law constants, reaction equilibrium constants, and thermodynamic parameters of SO_2 absorption in C_2mimCl-7 + AmPyr DESs

Parameters	293.15 K	303.15 K	313.15 K	333.15 K
H (bar)	0.10814 ± 0.00279	0.21585 ± 0.00688	0.30983 ± 0.01596	0.66939 ± 0.16117
$k_{\mathrm{C_2mimCl}}$	173.03801 ± 72.62040	99.15970 ± 14.25614	36.28764 ± 2.19755	15.10983 ± 0.82593
k_{AmPyr}	1.27796 ± 0.09255	1.11052 ± 0.05036	0.80265 ± 0.04400	0.46775 ± 0.06859
$R_5{}^2$	0.999	0.999	0.999	0.999
$\Delta_{\mathrm{phys}}H_{\mathrm{m}}$ (kJ mol^{-1})	−35.993	−35.993	−35.993	−35.993
$\Delta_{\mathrm{phys}}G_{\mathrm{m}}$ (kJ mol^{-1})	−5.421	−3.864	−3.051	−1.112
$\Delta_{\mathrm{phys}}S_{\mathrm{m}}$ (J mol K^{-1})	−104.287	−105.983	−105.197	−104.701
$\Delta_{\mathrm{chem}}H_{\mathrm{m}}$ (kJ mol^{-1})	−72.131	−72.131	−72.131	−72.131
$\Delta_{\mathrm{chem}}G_{\mathrm{m}}$ (kJ mol^{-1})	−13.158	−11.850	−8.779	−5.416
$\Delta_{\mathrm{chem}}S_{\mathrm{m}}$ (J mol K^{-1})	−201.169	−198.85	−202.308	−200.254
$\Delta_{\mathrm{r}}H_{\mathrm{m}}$ (kJ mol^{-1})	−108.124	−108.124	−108.124	−108.124
$\Delta_{\mathrm{r}}G_{\mathrm{m}}$ (kJ mol^{-1})	−18.579	−15.714	−11.829	−6.528
$\Delta_{\mathrm{r}}S_{\mathrm{m}}$ (J mol K^{-1})	−305.457	−304.833	−307.505	−304.955

$m_{\mathrm{phys\text{-}SO_2}}$ is most significantly controlled by temperature, followed by $m_{\mathrm{AmPyr\text{-}SO_2}}$, and $m_{\mathrm{C_2mimCl\text{-}SO_2}}$ is least affected, indicating that the interaction between C_2mimCl and SO_2 is stronger than AmPyr, and the physical interaction is the weakest. Besides, the physical absorption capacity increases linearly with increasing pressure, while the chemical absorption capacity increases nonlinearly and gradually approaches equilibrium. Thus, the absorption capacity of DESs for SO_2 gradually increases linearly with the increase of pressure.

According to the relationship of $\ln H$ and $\ln k$ to $1/T$ (Fig. 4a), the parameters of enthalpy change (ΔH_{m}), Gibbs free energy change (ΔG_{m}), and entropy change (ΔS_{m}) could be obtained by the following equations:

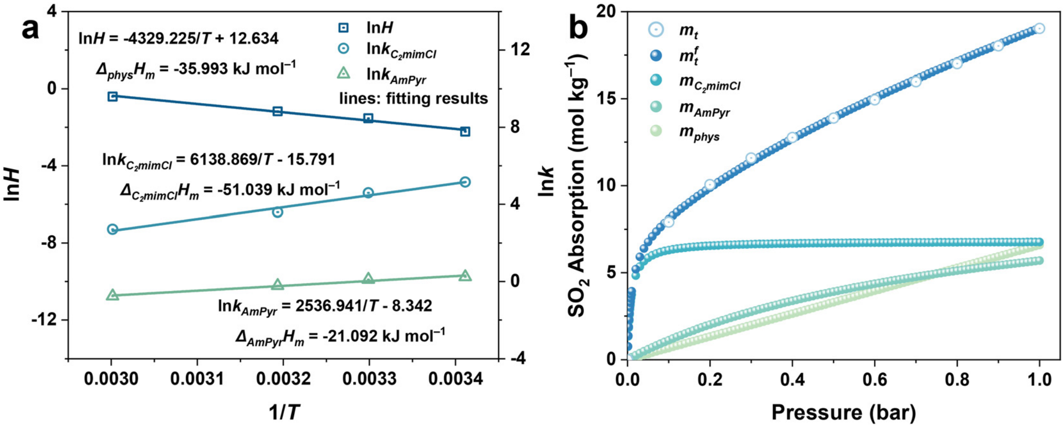

Fig. 4 (a) The fitting results of $\ln H$ and $\ln k$ to $1/T$ of C_2mimCl-7 + AmPyr; (b) the calculated SO_2 absorption of C_2mimCl-7 + AmPyr at 298.15 K.

$$\Delta_{\text{phys}}H_{\text{m}} = R\left(\frac{\partial \ln H_{\text{m}}}{\partial(1/T)}\right) \tag{13}$$

$$\Delta_{\text{phys}}G_{\text{m}} = RT\ln H_{\text{m}} \tag{14}$$

$$\Delta_{\text{phys}}S_{\text{m}} = \frac{\Delta_{\text{phys}}H_{\text{m}} - \Delta_{\text{phys}}G_{\text{m}}}{T} \tag{15}$$

$$\Delta_{\text{C}_2\text{mimCl}}H_{\text{m}} = -R\left(\frac{\partial \ln k_{\text{C}_2\text{mimCl}}}{\partial(1/T)}\right) \tag{16}$$

$$\Delta_{\text{AmPyr}}H_{\text{m}} = -R\left(\frac{\partial \ln k_{\text{AmPyr}}}{\partial(1/T)}\right) \tag{17}$$

$$\Delta_{\text{chem}}H_{\text{m}} = \Delta_{\text{C}_2\text{mimCl}}H_{\text{m}} + \Delta_{\text{AmPyr}}H_{\text{m}} \tag{18}$$

$$\Delta_{\text{chem}}G_{\text{m}} = -RT(\ln k_{\text{C}_2\text{mimCl}} + \ln k_{\text{AmPyr}}) \tag{19}$$

$$\Delta_{\text{chem}}S_{\text{m}} = \frac{\Delta_{\text{chem}}H_{\text{m}} - \Delta_{\text{chem}}G_{\text{m}}}{T} \tag{20}$$

Here, $\Delta_{\text{phys}}H_{\text{m}}$, $\Delta_{\text{phys}}G_{\text{m}}$, and $\Delta_{\text{phys}}S_{\text{m}}$ correspond to the physical process; $\Delta_{\text{C}_2\text{mimCl}}H_{\text{m}}$, $\Delta_{\text{AmPyr}}H_{\text{m}}$, $\Delta_{\text{chem}}H_{\text{m}}$, $\Delta_{\text{chem}}G_{\text{m}}$, and $\Delta_{\text{chem}}S_{\text{m}}$ correspond to the chemical process (Table 2). As can be seen, the values of ΔH_{m}, ΔG_{m}, and ΔS_{m} are always less than 0, which indicate the absorption process is exothermic, spontaneous, and with increased orderliness.

Besides, the $\ln H$, $\ln k_{\text{C}_2\text{mimCl}}$, and $\ln k_{\text{AmPyr}}$ at 298.15 K can be calculated, and the SO_2 absorption of m_{phys}, $m_{\text{C}_2\text{mimCl}}$, m_{AmPyr}, and m_{t}^{f} could be further obtained. Fig. 4b shows that the calculated SO_2 absorption remains consistent with the experimental values (such as 19.051 mol kg^{-1} *vs.* 19.032 mol kg^{-1} at 1.0 bar), indicating the high reliability of the DS-RETM equation.

To further investigate the absorption behavior of different pyrimidine-based DESs, $m^{\circ}_{\text{C}_2\text{mimCl}}$ and m°_{AmPyr} in eqn (12) were replaced with the initial molality of the corresponding HBAs and HBDs (m°_{HBAs} and m°_{HBDs}), resulting in DS-RETM equations for different HBAs-7 + HBDs DESs. Subsequently, the SO_2 absorption of different pyrimidine-based DESs at 298.15 K was fitted, and the detailed results are shown in Fig. S2 and Table S9. Based on the obtained H, k_{HBAs}, and k_{HBDs}, the m_{phys}, m_{HBAs}, and m_{HBDs} of corresponding HBAs-7 + HBDs DESs could be calculated separately, which is of great significance for insight exploration of the absorption behavior of each component in DESs (Fig. S3). Compared with C_2mimBr-7 + AmPyr, the m_{HBDs}, m_{HBAs}, and m_{phys} of C_2mimCl-7 + AmPyr were significantly increased, indicating that Cl^- has a key impact on the SO_2 absorption of DESs. Obviously, for DESs using the same HBAs (C_2mimCl-7 + HBDs), there is not much difference in m_{HBAs} (also known as $m_{\text{C}_2\text{mimCl}}$) (Fig. S3a and b), attributed to the same molar mass of C_2mimCl, which forms a strong charge transfer interaction between Cl^- and the S atom of SO_2 ($Cl^- \cdots SO_2$). However, significant differences in m_{HBDs} and m_{phys} between C_2mimCl-7 + HBDs DESs could be observed. Notably, the order of m_{HBDs} is not the same as the SO_2 absorption of their corresponding DESs (Fig. S3c and d). Among them, m_{AmPd} and m_{DAmPyr} are both greater than m_{AmPyr}, but the SO_2 absorption of C_2mimCl-7 + AmPyr is greater than that of C_2mimCl-7 + AmPd and C_2mimCl-7 + DAmPyr. Interestingly, for the physical absorption (m_{phys}) of C_2mimCl-7 + HBDs (Fig. S3e and f), there is even a phenomenon opposite to the SO_2 absorption of the corresponding DESs. For instance, C_2mimCl-7 + BrPyr has the minimum SO_2 absorption but the maximum m_{phys}. To sum up, the types and numbers of functional groups in HBDs determine their varying abilities to absorb SO_2, while also affecting the physical absorption properties of the corresponding DESs. Hence, DS-RETM fitting could visualize these potential absorption behaviors, which is more conducive to exploring the physical and chemical absorption processes of the prepared DESs.

2.4 Kinetic analysis of SO_2 absorption for pyrimidine-based DESs

A typical time-dependent SO_2 absorption process involves taking a certain amount of DESs (~0.10 g) and observing the change in SO_2 absorption capacity over time at an initial pressure of ~1.0 bar. The time-dependent SO_2 absorption capacity of C_2mimCl-7 + HBDs at 298.15 K is shown in Fig. 5a. Interestingly, the as-prepared DESs can absorb SO_2 rapidly, which suggests that the absorption process is mainly dominated by chemical absorption. To further observe the SO_2 absorption rate, Boltzmann equation (eqn (21)) fitting was performed on the experimental results,[32] and the first derivative of the curve is the absorption rate of the as-prepared pyrimidine-based DESs (Fig. 5b). Clearly, C_2mimCl-7 + AmPyr achieved the maximum absorption rate in the shortest possible time. Moreover, the as-prepared DESs can rapidly absorb SO_2 and basically achieve absorption equilibrium within 40 s, which is superior to numerous reported DESs.[35,49–51] This result shows that pyrimidine-based DESs have potential for flue gas desulfurization.

$$m_{\text{SO}_2} = \frac{A_1 - A_2}{1 + \text{e}^{(t - t_0)/\text{d}t}} + A_2 \tag{21}$$

where m_{SO_2} refers to the SO_2 absorption capacity (mol kg^{-1}), t refers to the time of SO_2 absorption (s), and A_1, A_2, t_0, and d_{t} refer to the empirical constants.

2.5 SO_2/CO_2 absorption selectivity of pyrimidine-based DESs

Owing to the complex composition of actual flue gas, it generally contains 0.04–15% CO_2.[52] Thus, the designed absorbent for flue gas desulfurization should have high SO_2/CO_2 selectivity. The CO_2 and SO_2 absorption capacities of C_2mimCl-7 + HBDs were compared at 298.15 K and 1.0 bar, as shown in Fig. 6. Obviously, pyrimidine-based DESs show a negative absorption of CO_2. Generally, the selectivity of SO_2/CO_2 keeps the ratio of SO_2 absorption capacity to CO_2 absorption capacity under given conditions

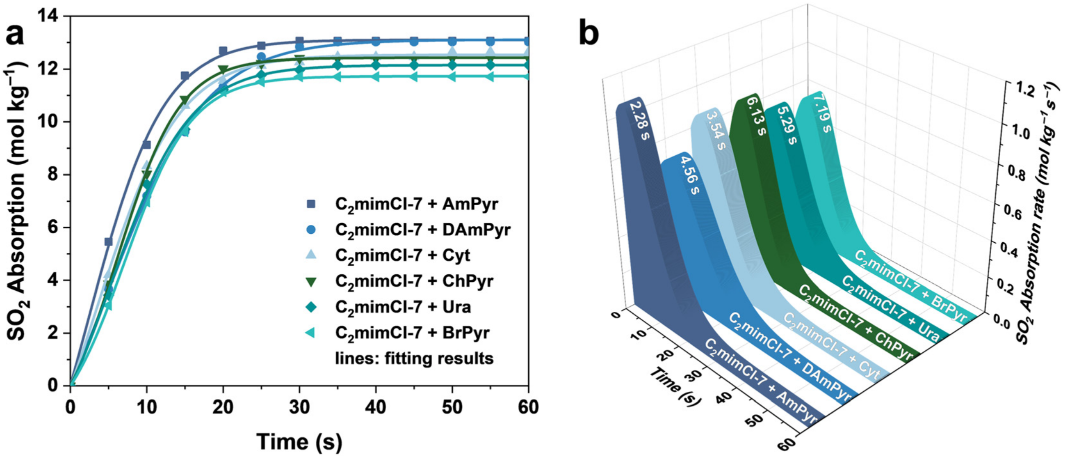

Fig. 5 (a) The time-dependent SO_2 absorption and (b) SO_2 absorption rate of pyrimidine-based DESs; T = 298.15 K.

($S_{\mathrm{DESs}} = m_{SO_2}/m_{CO_2}$).[29] The comparison of SO_2 absorption capacity and selectivity with literature data is shown in Table S10. Accordingly, the absorption selectivity of pyrimidine-based DESs is C_2mimCl-7 + ChPyr (451.6), C_2mimCl-7 + Ura (494.2), C_2mimCl-7 + AmPyr (528.7), C_2mimCl-7 + BrPyr (536.5), C_2mimCl-7 + DAmPyr (808.5), C_2mimCl-7 + Cyt (1073.1), respectively. The minimum value of S_{DESs} has reached up to 451.6, indicating that pyrimidine-based DESs have excellent SO_2/CO_2 selective absorption performance and could be used as a candidate for selective absorption of SO_2 from actual flue gas.

2.6 SO_2 absorption mechanism of pyrimidine-based DESs

To explore the mechanism of DES formation and SO_2 absorption, C_2mimCl-7 + AmPyr with the highest absorption capacity was selected for FT-IR and ^{1}H NMR analysis. In Fig. 7a, the peaks appearing at 3325 and 3161 cm^{-1} are attributed to the stretching vibration of $-N_{(g)}H_2$, the peak around 1645 cm^{-1} is attributed to the bending vibration of $-N_{(g)}H_2$, and two peaks at 1575 and 1556 cm^{-1} are attributed to the stretching vibration of the pyrimidine ring.[53] In DES (C_2mimCl-7 + AmPyr), the peak of $-N_{(g)}H_2$ around 1645 cm^{-1} is red shifted to 1628 cm^{-1}, indicating that AmPyr had hydrogen bond interactions with C_2mimCl ($N_{(g)}-H\cdots Cl^-$). Besides, the peak of $C_{(2)}-H$ in C_2mimCl around 3056 cm^{-1} shifts to 3046 cm^{-1},[51] which may be due to Cl^- forming intramolecular hydrogen bonds ($C_{(2)}-H\cdots Cl^-$), leading to a decrease in force constant and vibrational energy, and a red shift in functional groups.[23,29,54]

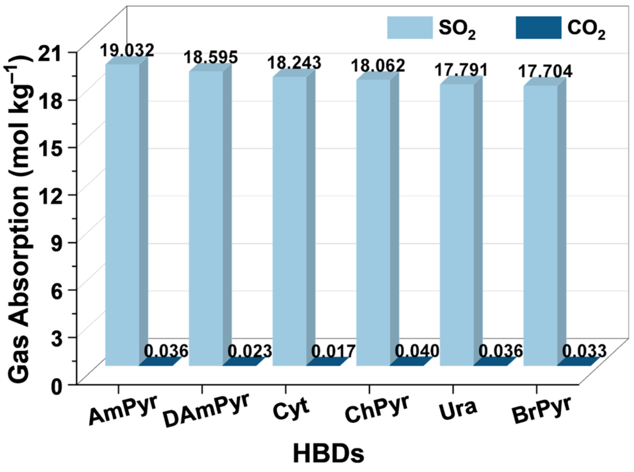

Fig. 6 The gas absorption of C_2mimCl-7 + HBDs; T = 298.15 K, P = 1.0 bar.

For the spectrum after SO_2 absorption, four new peaks attributed to SO_2 could be observed. Among them, three peaks are attributed to the bending vibration (529 cm^{-1}), symmetric stretching vibration (1124 cm^{-1}), and asymmetric stretching vibration (1281 cm^{-1}) of S=O, respectively.[6,22,32] Compared with free SO_2, a significant red shift was observed in the stretching vibration of S=O, indicating that Cl^- in C_2mimCl may form a charge transfer interaction with S atoms in SO_2 ($Cl^-\cdots SO_2$).[55,56] Hence, the original hydrogen bonds in DESs get weakened significantly, leading to the peaks of $-C_{(8)}H_3$, $C_{(2)}-H$ and $C_{(4+5)}-H$ shifting from 2976, 3046 and 3140 cm^{-1} to 2984, 3088 and 3145 cm^{-1}, respectively.[32,49] The fourth peak around 836 cm^{-1} is attributed to the bending vibration of S–O, indicating that there exists chemical absorption of SO_2.[28,57] Owing to the bending vibration of $-N_{(g)}H_2$ shifting and splitting into two peaks around 1693 and 1680 cm^{-1}, it is inferred that the acid–base interactions might be formed between AmPyr and SO_2.[23] Contrary to SO_2 absorption, the FT-IR spectrum after CO_2 absorption showed no significant changes compared to before absorption, indicating that there is almost no interaction between the as-prepared DESs and CO_2, thus exhibiting extremely high SO_2/CO_2 selectivity.

Fig. 7b shows the ^{1}H NMR spectra of AmPyr, C_2mimCl, C_2mimCl-7 + AmPyr, and C_2mimCl-7 + AmPyr after SO_2 absorption. Notably, the peak of $-N_{(g)}H_2$ shifts from 6.59 ppm in AmPyr to 6.66 ppm in DES, and the peak of $C_{(2)}-H$ shifts from 9.70 ppm in C_2mimCl to 9.78 ppm in DES.

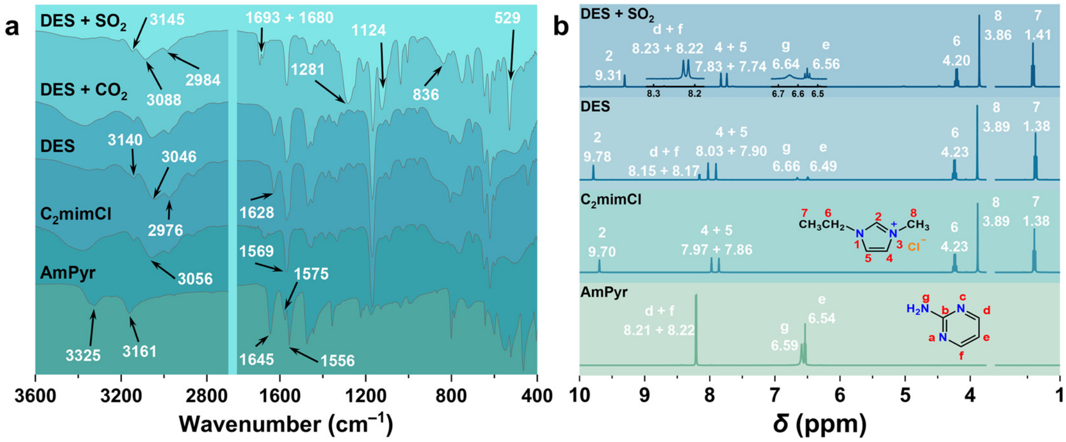

Fig. 7 (a) FT-IR spectra of C_2mimCl-7 + AmPyr after SO_2 absorption (DES + SO_2), C_2mimCl-7 + AmPyr after CO_2 absorption (DES + CO_2), C_2mimCl-7 + AmPyr (DES), C_2mimCl and AmPyr; (b) ^{1}H NMR spectra of DES + SO_2, DES, C_2mimCl and AmPyr.

These down-field shifts are attributed to the formation of $N_{(g)}$–H⋯Cl^- and $C_{(2)}$–H⋯Cl^-,[23] respectively, which would reduce electron cloud density (de-shielding effect).[25,58] Concurrently, the peak of $C_{(4+5)}$–H shifts to down-field, while the peaks of $C_{(d+f)}$–H and $C_{(e)}$–H shift to up-field. In contrast, the peaks of $C_{(2)}$–H and $-N_{(g)}H_2$ shift to up-field after SO_2 absorption. The former is attributed to the charge transfer between the Cl^- and S atoms ($Cl^-\cdots SO_2$), while the latter could be ascribed to the acid–base interaction between $-N_{(g)}H_2$ and SO_2.[25,59] The shift of other C–H signals in C_2mimCl and AmPyr indicates that the original hydrogen bonds in DES have been disrupted by SO_2.

2.7 Regeneration of pyrimidine-based DESs

In order to avoid secondary pollution caused by a large number of waste absorbents, it is usually required that the absorbents have good regeneration performance. As shown in Fig. 8, C_2mimCl-7 + AmPyr maintains the SO_2 absorption capacity of 18.265 mol kg^{-1} after 30 times of absorption–desorption. This represents excellent regeneration performance compared with the reported DESs for absorbing SO_2.[16,22,23,38,60] To investigate whether the structure of pyrimidine-based DESs is stable and maintains the original absorption performance, the SO_2 absorption capacity of C_2mimCl-7 + AmPyr was measured every 7 days under the same conditions (Fig. S4). The results showed that C_2mimCl-7 + AmPyr remained liquid after 4 weeks, and maintained excellent SO_2 absorption performance.

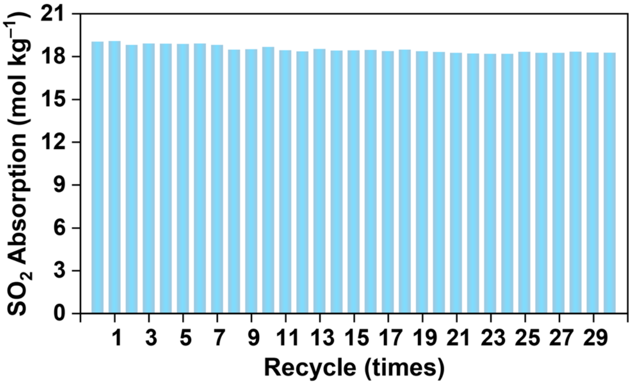

Fig. 8 The regeneration performance of C_2mimCl-7 + AmPyr.

3 Conclusions

In this work, 14 different DESs were successfully developed and used for SO_2 absorption. The density and viscosity of the as-prepared DESs show a negative correlation with temperature, but the former is linear and the latter is exponential. As the molar ratio of C_2mimCl to AmPyr increases, the SO_2 absorption capacity of C_2mimCl-*n* + AmPyr gradually increases, ultimately reaching up to 19.032 mol kg^{-1} at 298.15 K and 1.0 bar. The thermodynamic analysis of SO_2 absorption by C_2mimCl-7 + AmPyr at different temperatures was conducted using the DS-RETM equation, which not only yielded a series of thermodynamic parameters, but also successfully calculated the SO_2 absorption capacity (19.051 mol kg^{-1}) that is highly consistent with the experimental values at 298.15 K, indicating that this model has extremely high reliability. Subsequently, it was further applied to analyze the absorption behavior of C_2mimCl-7 + HBDs DESs, and the corresponding m_{phys}, $m_{\mathrm{C_2mimCl}}$, and m_{HBDs} were obtained, demonstrating the impact of different HBDs on SO_2 absorption. Dynamics analysis shows that the as-prepared DESs could reach gas–liquid equilibrium in 40 s. Besides, the present DESs exhibit remarkable SO_2/CO_2 selectivity, with C_2mimCl-7 + AmPyr achieving a value as high as 528.7. After 30 cycles of absorption–desorption, the SO_2 absorption of the regenerated C_2mimCl-7 + AmPyr still reached 18.265 mol kg^{-1}. Finally, combining thermodynamic analysis, FT-IR, and ^{1}H NMR results, it is indicated that the SO_2 absorption process involves physical absorption and chemical absorption.

4 Experimental section

Preparation of DESs: C_2mimCl-*n* + AmPyr DESs (*n* = 2, 3, 4, 5, 6, and 7) were prepared by combining C_2mimCl and AmPyr at specified molar ratios (2 : 1, 3 : 1, 4 : 1, 5 : 1, 6 : 1, 7 : 1). The mixtures underwent heating at 353.15 K for 180 min with constant stirring. Subsequent cooling to ambient temperature yielded homogeneous liquids (Scheme S2).

C_2mimCl-7 + ChPyr, C_2mimCl-7 + BrPyr, C_2mimCl-7 + Cyt, C_2mimCl-7 + DAmPyr, C_2mimCl-7 + Ura, C_2mimCl-7 + AmPd and C_2mimCl-7 + AmPz were prepared using 2-chloropyrimidine, 2-bromopyrimidine, 4-amino-2-hydroxypyrimidine, 4,6-diaminopyrimidene, 2,4-dihydroxypyrimidine, 3-aminopyridazine and 2-aminopyrazine as HBDs, respectively.

C_2mimBr-7 + AmPyr was prepared using C_2mimBr as a HBA and AmPyr as a HBD.

At a molar ratio of 7 : 1 and 353.15 K, with C_2mimCl as a HBA and TAmPyr as a HBD, DESs could not be formed after vigorous stirring at 800 rpm for 180 min.

For other details not described, please refer to the SI.

Conflicts of interest

There are no conflicts to declare.

Data availability

The data that support the findings of this study are available from the corresponding author upon reasonable request.

Supplementary information (SI) is available. See DOI: https://doi.org/10.1039/d5im00317b.

Acknowledgements

All authors appreciate the financial support from the National Science Foundation for Distinguished Young Scholars (No. 22425808), the National Natural Science Foundation of China (No. 22178154, 22578187), the Science Foundation of China University of Petroleum, Beijing (No. 2462022YJRC002, 2462022YJRC003), and the Carbon Neutrality Research Institute Fund (No. CNIF20240103).

References

1 W. Li, J. Li, T. D. Duong, S. A. Sapchenko, X. Han, J. D. Humby, G. F. S. Whitehead, I. J. Victórica-Yrezábal, I. da Silva, P. Manuel, M. D. Frogley, G. Cinque, M. Schröder and S. Yang, Adsorption of sulfur dioxide in Cu(II)-carboxylate framework materials: The role of ligand functionalization and open metal sites, *J. Am. Chem. Soc.*, 2022, **144**, 13196–13204.

2 X. Bie, R. Wu, B. Yu, X. Quan, S. Zhang, Q. Li, Y. Zhang and H. Zhou, Deactivation mechanisms of Cu–Zn–Al_2O_3 in CO_2 hydrogenation induced by SO_2 exposure, *Ind. Chem. Mater.*, 2025, **3**, 710–722.

3 X. Cao, Y. Liu, Q. Huang, Z. Chen, J. Sun, J. Sun, S. Pang, P. Liu, W. Wang, Y. Zhang and M. Ge, Single droplet tweezer revealing the reaction mechanism of Mn(II)-catalyzed SO_2 oxidation, *Environ. Sci. Technol.*, 2024, **58**, 5068–5078.

4 W. Zhao, J. L. Obeso, V. B. López-Cervantes, M. Bahri, E. Sánchez-González, Y. A. Amador-Sánchez, J. Ren, N. D. Browning, R. A. Peralta, G. Barcaro, S. Monti, D. Solis-Ibarra, I. A. Ibarra and D. Zhao, Achieving sub-ppm sensitivity in SO_2 detection with a chemically stable covalent organic framework, *Angew. Chem., Int. Ed.*, 2024, **64**, e202415088.

5 W. Gong, P. Gao, Y. Gao, Y. Xie, J. Zhang, X. Tang, K. Wang, X. Wang, X. Han, Z. Chen, J. Dong and Y. Cui, Modulator-directed counterintuitive catenation control for crafting highly porous and robust metal–organic frameworks with record high SO_2 uptake capacity, *J. Am. Chem. Soc.*, 2024, **146**, 31807–31815.

6 Q. Zhu, C. Wang, J. Yin, H. Li, W. Jiang, J. Liu, P. Li, Q. Zhang, Z. Chen and W. Zhu, Efficient and remarkable SO_2 capture: A discovery of imidazole-based ternary deep eutectic solvents, *J. Mol. Liq.*, 2021, **330**, 115595.

7 Z. Yan, S. Y. Lai, C. L. Ngan, H. Li and A. R. Mohamed, Recent advances in energy-efficient and regenerative SO_2 absorption over deep eutectic solvents, *J. Environ. Chem. Eng.*, 2022, **10**, 108967.

8 A. P. Abbott, G. Capper, D. L. Davies, R. K. Rasheed and V. Tambyrajah, Novel solvent properties of choline chloride/urea mixtures, *Chem. Commun.*, 2003, 70–71.

9 Y. Chen and Z. Yu, Low-melting mixture solvents: Extension of deep eutectic solvents and ionic liquids for broadening green solvents and green chemistry, *Green Chem. Eng.*, 2024, **5**, 409–417.

10 M. Hu, B. Han, L. Xie, B. Lu, D. Bai, N. Shi, Y. Liao, Y. Wang, L. Liu, S. Wu, R. Lan, X. Lei, C. Shi, D. Huang, Y. Li, L. Lin and J. Zhang, Ultrasonic assisted natural deep eutectic solvents as a green and efficient approach for extraction of hydroxytyrosol from olive leaves, *Ind. Chem. Mater.*, 2024, **2**, 309–320.

11 Y. Chen, G. Zhao, J. Dong, J. Wang, D. Dong, Z. Li, M. Zhao, Z. Shi and Z. Niu, Green recovery of all-solid-state sodium-ion batteries/lithium-ion batteries by ionic liquids, deep eutectic solvents and low-melting mixture solvents, *Ind. Chem. Mater.*, 2025, **3**, 464–474.

12 E. L. Smith, A. P. Abbott and K. S. Ryder, Deep eutectic solvents (DESs) and their applications, *Chem. Rev.*, 2014, **114**, 11060–11082.

13 M. Francisco, A. van den Bruinhorst and M. C. Kroon, Low-transition-temperature mixtures (LTTMs): A new generation of designer solvents, *Angew. Chem., Int. Ed.*, 2013, **52**, 3074–3085.

14 D. Yang, M. Hou, H. Ning, J. Zhang, J. Ma, G. Yang and B. Han, Efficient SO_2 absorption by renewable choline chloride–glycerol deep eutectic solvents, *Green Chem.*, 2013, **15**, 2261.

15 D. Deng, X. Liu and B. Gao, Physicochemical properties and investigation of azole-based deep eutectic solvents as efficient and reversible SO_2 absorbents, *Ind. Eng. Chem. Res.*, 2017, **56**, 13850–13856.

16 K. Zhang, S. Ren, X. Yang, Y. Hou, W. Wu and Y. Bao, Efficient absorption of low-concentration SO_2 in simulated flue gas by functional deep eutectic solvents based on imidazole and its derivatives, *Chem. Eng. J.*, 2017, **327**, 128–134.

17 D. Lee, W. Y. Choi, K. Jang, J. Park and Y. Yoo, Functionalized imidazole–alkanolamine deep eutectic solvents with remarkable performance for low-concentration SO_2 absorption, *Sep. Purif. Technol.*, 2023, **307**, 122782.

18 X. Li, L. Meng, F. Yang, Z. Yang, J. Li, Y. Chen and X. Ji, Tuning the structure of N-methyldiethanolamine-based deep eutectic solvents for efficient and reversible SO_2 capture, *Chem. Commun.*, 2024, **60**, 10560–10563.

19 G. Long, C. Yang, X. Yang, T. Zhao, F. Liu and J. Cao, Bisazole-based deep eutectic solvents for efficient SO_2 absorption and conversion without any additives, *ACS Sustainable Chem. Eng.*, 2020, **8**, 2608–2613.

20 L. Zhang, H. Ma, G. Wei, B. Jiang, Y. Sun, X. Tantai, Z. Huang and Y. Chen, Efficient and reversible nitric oxide absorption by low-viscosity, azole-derived deep eutectic solvents, *J. Chem. Eng. Data*, 2019, **64**, 3068–3077.

21 Y. Chen, B. Jiang, H. Dou, L. Zhang, X. Tantai, Y. Sun and H. Zhang, Highly efficient and reversible capture of low partial pressure SO_2 by functional deep eutectic solvents, *Energy Fuels*, 2018, **32**, 10737–10744.

22 P. Zhang, G. Xu, M. Shi, Z. Wang, Z. Tu, X. Hu, X. Zhang and Y. Wu, Unexpectedly efficient absorption of low-concentration SO_2 with phase-transition mechanism using deep eutectic solvent consisting of tetraethylammonium chloride and imidazole, *Sep. Purif. Technol.*, 2022, **286**, 120489.

23 Q. Wang, H. Wu, T. Zhang, Y. Fan, W. Zhang and K. He, Efficient absorption of low partial pressure SO_2 by deep eutectic solvents based on pyridine derivatives, *Chem. Eng. Res. Des.*, 2022, **177**, 36–44.

24 Z. Wang and D. Yang, SO_2 capture by 2-pyridineethanol through the formation of a zwitterionic liquid, *Chem. Commun.*, 2022, **58**, 6212–6214.

25 C. Wang, H. Wu, J. Li, J. Zhang, J. Zhang, J. Ding, H. Li, H. Li and W. Zhu, Surpassingly efficient, selective, and reversible absorption of SO_2 through pyridine based deep eutectic solvents, *Chem. Eng. J.*, 2023, **471**, 144394.

26 T. Yang, Y. Wang, Z. Huang, F. Liu, Q. Liao and T. Zhao, Deep eutectic solvents composed of 1-methyl-3-ethylimidazole halides and pyridine derivatives for efficient absorption and conversion of SO_2 into cyclic sulfites under ambient conditions, *Sep. Purif. Technol.*, 2025, **361**, 131475.

27 P. Zhang, Z. Tu, X. Zhang, X. Hu and Y. Wu, Acidic protic ionic liquid-based deep eutectic solvents capturing SO_2 with low enthalpy changes, *AIChE J.*, 2023, **69**, e18145.

28 Y. Zou, C. Wang, H. Ji, P. Wu, Y. Chao, X. Yu, Z. Yu, H. Liu, Z. Liu and W. Zhu, Rapid, selectivity, and reversibility absorption of SO_2 via purine-based deep eutectic solvents and thermodynamic analysis, *Green Chem. Eng.*, 2026, **7**, 180–190.

29 P. Li, X. Wang, T. Zhao, C. Yang, X. Wang and F. Liu, Deep eutectic solvents formed by EmimCl plus lactams: Effective SO_2 capture and conversion into sulphur via DESs-mediated claus process, *Chem. Eng. J.*, 2021, **422**, 130033.

30 X. Y. Luo, X. Fan, G. L. Shi, H. R. Li and C. M. Wang, Decreasing the viscosity in CO_2 capture by amino-functionalized ionic liquids through the formation of intramolecular hydrogen bond, *J. Phys. Chem. B*, 2016, **120**, 2807–2813.

31 M. Pan, Y. Zhao, X. Zeng and J. Zou, Efficient absorption of CO_2 by introduction of intramolecular hydrogen bonding in chiral amino acid ionic liquids, *Energy Fuels*, 2018, **32**, 6130–6135.

32 K. Sheng, D. Li and Y. Kang, Unexpectedly promoted SO_2 capture in novel ionic liquid-based eutectic solvents: The synergistic interactions, *J. Mol. Liq.*, 2021, **337**, 116432.

33 Y. Cao, J. Zhang, Y. Ma, W. Wu, K. Huang and L. Jiang, Designing low-viscosity deep eutectic solvents with multiple weak-acidic groups for ammonia separation, *ACS Sustainable Chem. Eng.*, 2021, **9**, 7352–7360.

34 G. Long, C. Yang, X. Yang, T. Zhao and M. Xu, Deep eutectic solvents consisting of 1-ethyl-3-methylimidazolium chloride and glycerol derivatives for highly efficient and reversible SO_2 capture, *J. Mol. Liq.*, 2020, **302**, 112538.

35 B. Jiang, H. Zhang, L. Zhang, N. Zhang, Z. Huang, Y. Chen, Y. Sun and X. Tantai, Novel deep eutectic solvents for highly efficient and reversible absorption of SO_2 by preorganization strategy, *ACS Sustainable Chem. Eng.*, 2019, **7**, 8347–8357.

36 X. Wu, R. Guan, W. Zheng and K. Huang, New deep eutectic solvents formed by 1-ethyl-3-methylimidazolium chloride and dicyandiamide: Physiochemical properties and SO_2 absorption performance, *J. Taiwan Inst. Chem. Eng.*, 2021, **119**, 45–51.

37 D. Deng, G. Han and Y. Jiang, Investigation of a deep eutectic solvent formed by levulinic acid with quaternary ammonium salt as an efficient SO_2 absorbent, *New J. Chem.*, 2015, **39**, 8158–8164.

38 C. Wang, G. Cui, X. Luo, Y. Xu, H. Li and S. Dai, Highly efficient and reversible SO_2 capture by tunable azole-based ionic liquids through multiple-site chemical absorption, *J. Am. Chem. Soc.*, 2011, **133**, 11916–11919.

39 Y. Jiang, X. Liu and D. Deng, Solubility and thermodynamic properties of SO_2 in three low volatile urea derivatives, *J. Chem. Thermodyn.*, 2016, **101**, 12–18.

40 D. Yang, Y. Han, H. Qi, Y. Wang and S. Dai, Efficient absorption of SO_2 by EmimCl-EG deep eutectic solvents, *ACS Sustainable Chem. Eng.*, 2017, **5**, 6382–6386.

41 K. Zhang, S. Ren, Y. Hou and W. Wu, Efficient absorption of SO_2 with low-partial pressures by environmentally benign functional deep eutectic solvents, *J. Hazard. Mater.*, 2017, **324**, 457–463.

42 G. Cui, J. Liu, S. Lyu, H. Wang, Z. Li and J. Wang, Efficient and reversible SO_2 absorption by environmentally friendly task-specific deep eutectic solvents of PPZBr + Gly, *ACS Sustainable Chem. Eng.*, 2019, **7**, 14236–14246.

43 Z.-M. Li, W.-Q. Gong, J.-F. Li, S.-X. Zhu, D.-J. Tao and Y. Zhou, Efficient and selective absorption of SO_2 by low-

viscosity matrine-based deep eutectic solvents, *J. Mol. Liq.*, 2022, **367**, 120521.

44 Y. Zhao, J. Dou, R. Dai, H. Bai, S. Khoshk Rish, X. Xiao and J. Yu, Superefficient absorption of low-concentration SO_2 in flue gas using new ternary imidazole-based deep eutectic solvents: Mechanism, thermodynamics, and process analysis, *Energy Fuels*, 2022, **36**, 8351–8359.

45 Y. Zhao, J. Dou, H. Li, R. Dai, H. Bai, S. Khoshk Rish, X. Chen, X. Xiao and J. Yu, Low-cost Na_2S-EG-MTPB deep eutectic solvents absorb SO_2 effectively at a high temperature in flue gas, *Sep. Purif. Technol.*, 2022, **303**, 122283.

46 T. Zhou, Y. Zhao, X. Xiao, Y. Liu, H. Bai, X. Chen, J. Dou and J. Yu, Effective absorption mechanism of SO_2 and NO_2 in the flue gas by ammonium-bromide-based deep eutectic solvents, *ACS Omega*, 2022, **7**, 29171–29180.

47 W. J. Jiang, F. Y. Zhong, L. S. Zhou, H. L. Peng, J. P. Fan and K. Huang, Chemical dual-site capture of NH_3 by unprecedentedly low-viscosity deep eutectic solvents, *Chem. Commun.*, 2020, **56**, 2399–2402.

48 P. Liu, K. Cai, X. Zhang, X. Wang, M. Xu, F. Liu and T. Zhao, Rich ether-based protic ionic liquids with low viscosity for selective absorption of SO_2 through multisite interaction, *Ind. Eng. Chem. Res.*, 2022, **61**, 5971–5983.

49 D. Yang, S. Zhang, D. E. Jiang and S. Dai, SO_2 absorption in EmimCl-TEG deep eutectic solvents, *Phys. Chem. Chem. Phys.*, 2018, **20**, 15168–15173.

50 T. Zhao, J. Liang, Y. Zhang, Y. Wu and X. Hu, Unexpectedly efficient SO_2 capture and conversion to sulfur in novel imidazole-based deep eutectic solvents, *Chem. Commun.*, 2018, **54**, 8964–8967.

51 M. Lv, D. Yang and J. Chen, Deep eutectic solvents consisting of 1-ethyl-3-methylimidazolium chloride and biobased 2-pyrrolidone for reversible SO_2 capture, *ChemistrySelect*, 2020, **5**, 7142–7147.

52 H. Wang, P. Wu, C. Li, J. Zhang and R. Deng, Reversible and efficient absorption of SO_2 with natural amino acid aqueous solutions: Performance and mechanism, *ACS Sustainable Chem. Eng.*, 2022, **10**, 4451–4461.

53 S. Akyüz and T. Akyüz, FT-IR spectroscopic investigations of surface and intercalated 2-aminopyrimidine adsorbed on sepiolite and montmorillonite from Anatolia, *J. Mol. Struct.*, 2003, **651–653**, 205–210.

54 C. Wang, Q. Bi, Y. Huo, Z. Zhang, D. Tao, Y. Shen, Q. Zhu, Z. Chen, H. Li and W. Zhu, Investigation of amine-based ternary deep eutectic solvents for efficient, rapid, and reversible SO_2 absorption, *Energy Fuels*, 2021, **35**, 20406–20410.

55 X. Yang, Y. Zhang, F. Liu, P. Chen, T. Zhao and Y. Wu, Deep eutectic solvents consisting of EmimCl and amides: Highly efficient SO_2 absorption and conversion, *Sep. Purif. Technol.*, 2020, **250**, 117273.

56 K.-Y. Lee, C.-S. Kim, H.-G. Kim, M.-S. Cheong, D. K. Mukherjee and K.-D. Jung, Effects of halide anions to absorb SO_2 in ionic liquids, *Bull. Korean Chem. Soc.*, 2010, **31**, 1937–1940.

57 Z. L. Li, L. S. Zhou, Y. H. Wei, H. L. Peng and K. Huang, Highly efficient, reversible, and selective absorption of SO_2 in 1-ethyl-3-methylimidazolium chloride plus imidazole deep eutectic solvents, *Ind. Eng. Chem. Res.*, 2020, **59**, 13696–13705.

58 W. S. Ham, H. Choi, J. Zhang, D. Kim and S. Chang, C_2-selective, functional-group-divergent amination of pyrimidines by enthalpy-controlled nucleophilic functionalization, *J. Am. Chem. Soc.*, 2022, **144**, 2885–2892.

59 C. Wang, J. Zhang, Y. Zou, J. Ding, H. Li, M. Zhang, H. Li and W. Zhu, Effects of attractive electrostatic interactions on sulfur dioxide capture by functionalized deep eutectic solvents with abundant negative sites, *Chem. Eng. J.*, 2025, **519**, 165030.

60 S. Sun, Y. Niu, Q. Xu, Z. Sun and X. Wei, Efficient SO_2 absorptions by four kinds of deep eutectic solvents based on choline chloride, *Ind. Eng. Chem. Res.*, 2015, **54**, 8019–8024.